

Neuron, Volume 81

Supplemental Information

**Flow of Cortical Activity Underlying
a Tactile Decision in Mice**

Zengcai V. Guo, Nuo Li, Daniel Huber, Eran Ophir, Diego Gutnisky, Jonathan T. Ting, Guoping Feng, and Karel Svoboda

A Experiment sequence

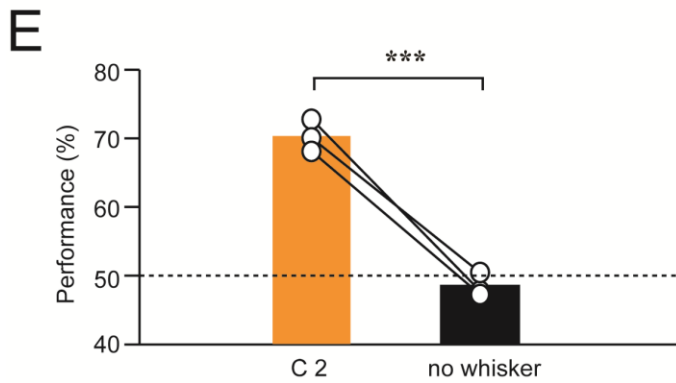
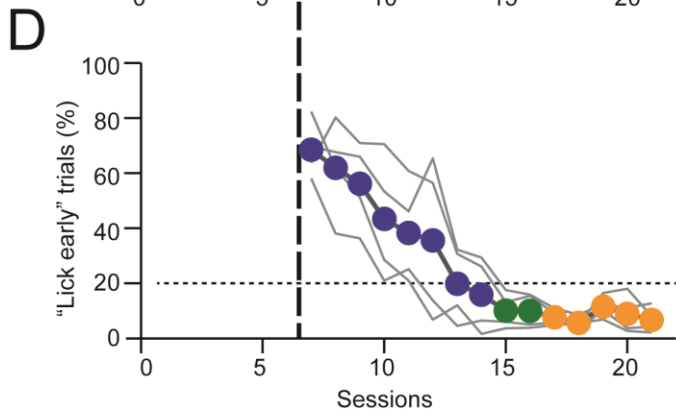
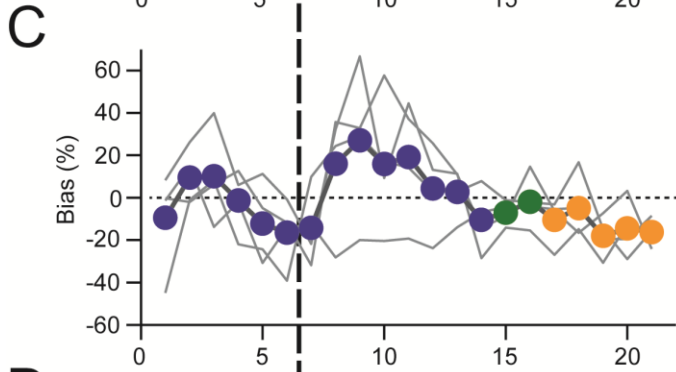
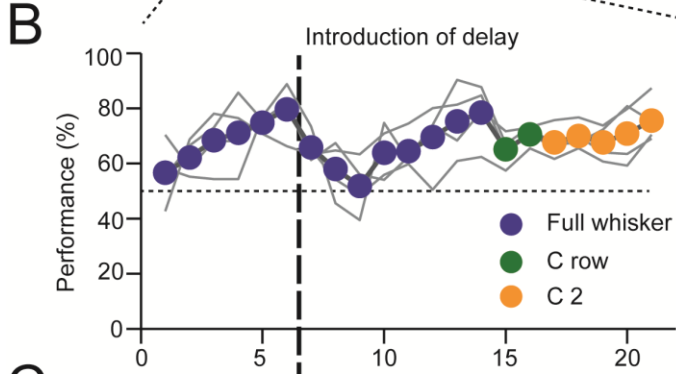
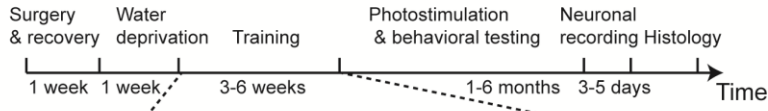


Figure S1 (related to Figure 1). Object location discrimination behavior.

- (A) Experimental time course.
- (B) Learning curves. Thick line, mean performance; thin lines, four individual mice; vertical dashed line, time of introduction of the delay epoch. Color changes indicate whisker trimming.
- (C) Response bias, defined as the performance in “lick right” trials minus the performance in “lick left” trials.
- (D) Fraction of aborted trials.
- (E) Object location discrimination requires whisker touch. After the mice were trained to perform the task with the C2 whisker, the C2 whisker was trimmed so that it was not able to reach the pole. Bars show mean performance in sessions before and after whisker trimming. Thin lines, three individual mice. ***, $p < 0.001$, two tailed t -test.

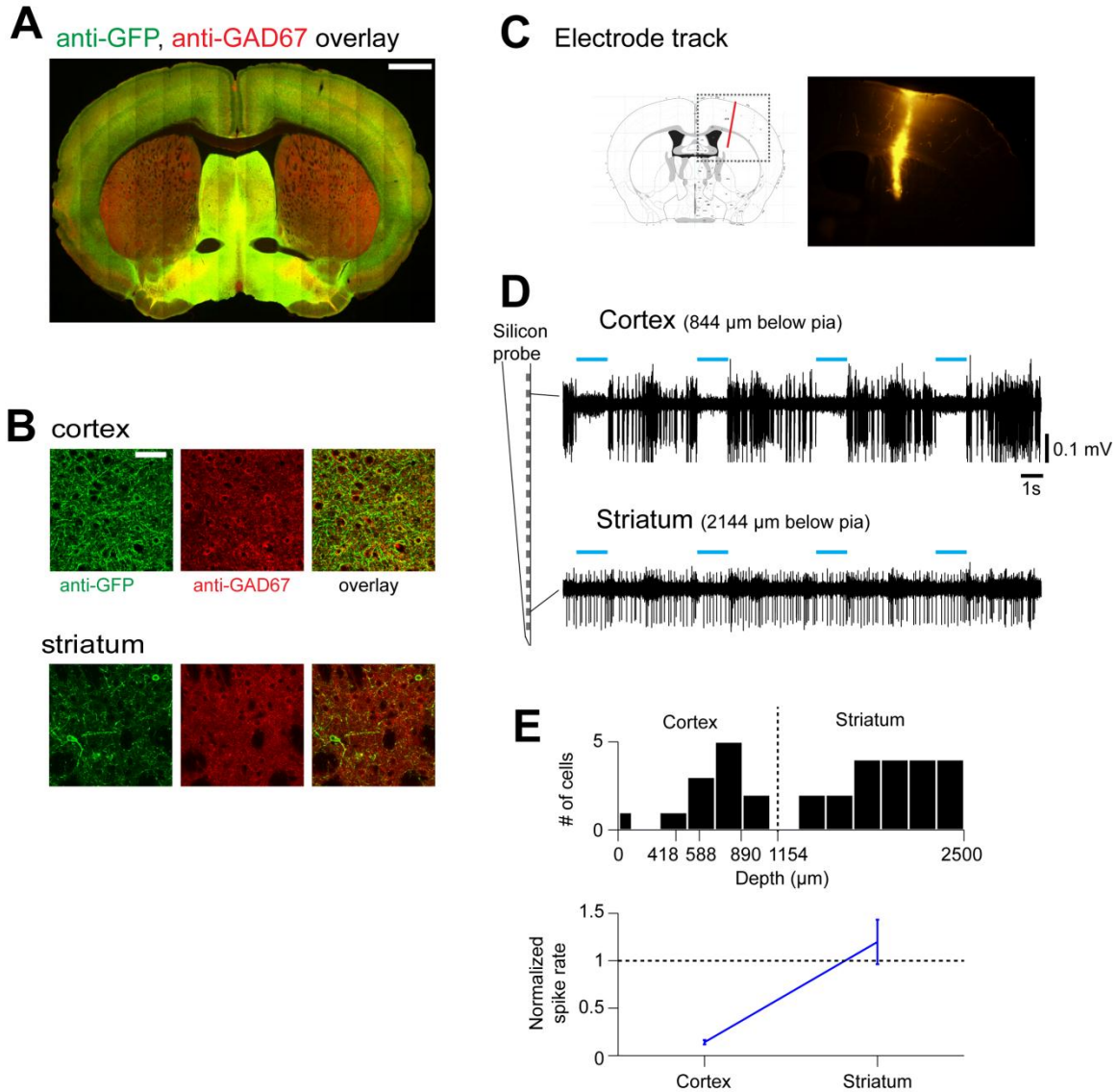


Figure S2 (related to Figure 2). Photostimulation of GABAergic neurons (photoinhibition) is limited to the cerebral cortex in *VGAT-ChR2-EYFP* mice.

- (A) Expression of ChR2-YFP in *VGAT-ChR2-EYFP* mice (Supplemental Experimental Procedures). Coronal section showing high ChR2-YFP expression in the neocortex and thalamus, but low expression in the striatum below neocortex. Scale bar, 1 mm.
- (B) High magnification images. The majority of GABAergic neurons express ChR2-YFP in the neocortex (>90%) (Zhao et al., 2011). In contrast, only a small fraction of neurons in the striatum express ChR2-YFP. Scale bar, 100 μm .
- (C) Recording experiments to confirm that photoinhibition did not directly affect striatum beneath neocortex. A long (3.2 mm) single shank silicon

- probe was inserted into the neocortex and striatum below. Sites along the electrode (100 μm spacing) simultaneously recorded activity from neocortex and striatum. *Left*, electrode track overlaid on a coronal section of a mouse brain (bregma -0.38 mm, Allen Brain Atlas). *Right*, electrode track marked with Dil (image corresponds to box on left).
- (D) Simultaneous recording from neocortex and striatum. Activity in neocortex was reduced by photoinhibition, whereas activity in striatum was unaffected.
- (E) Summary data from all simultaneously recorded neocortical units ($n = 12$) and striatal units ($n = 20$). *Top*, cell count as a function of recording depth. The bin around 1154 μm corresponds to the white matter. Neurons below 1154 μm are classified as striatal neurons. *Bottom*, normalized spike rate for neocortical putative pyramidal neurons and striatal neurons. Error bars show s.e.m. over neurons. Normalized spike rate for the striatal neurons are not significantly different from 1 ($p = 0.42$, t -test).

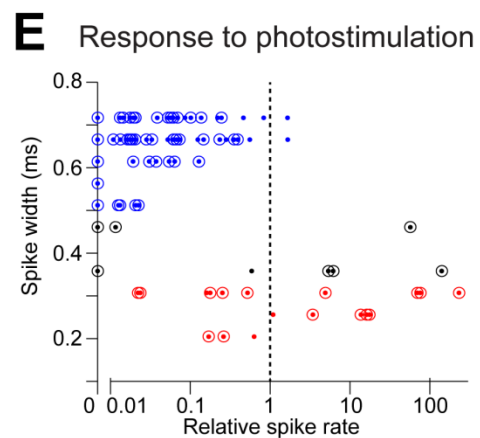
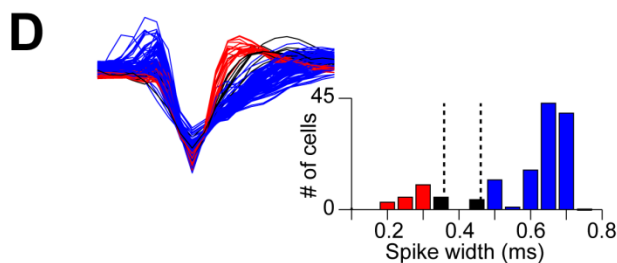
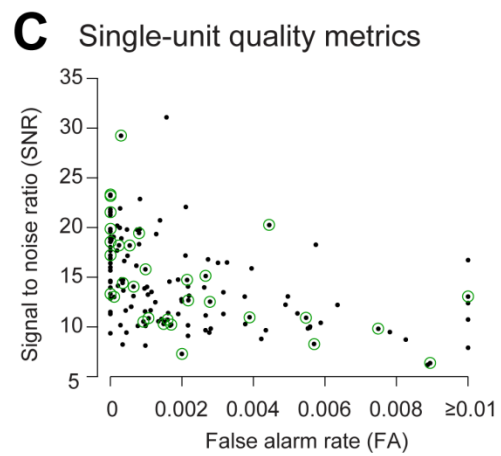
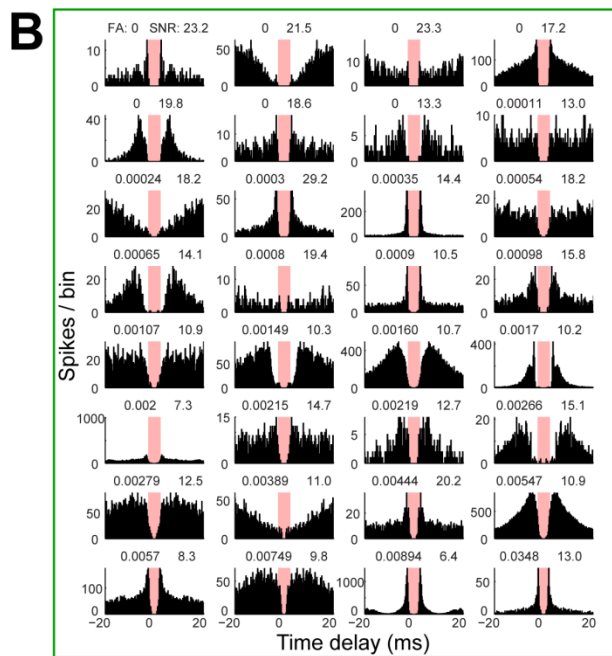
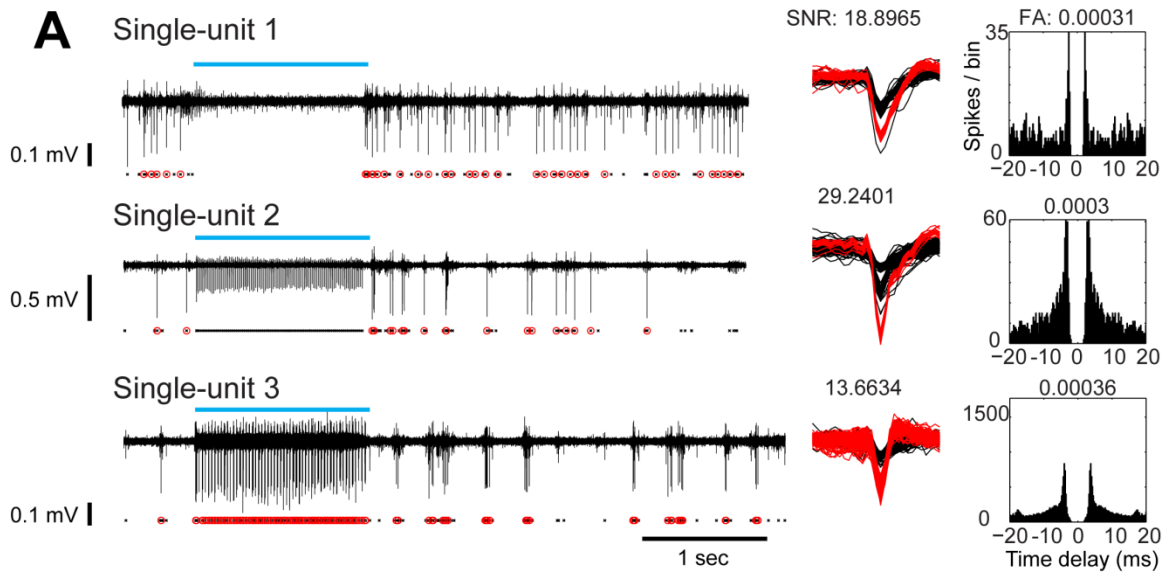


Figure S3 (related to Figure 2). Silicon probe recordings.

(A) Three example single units. *Left*, voltage traces. All detected events are shown as black ticks below the voltage traces. Spikes from the single units

- are highlighted in red. Blue bar indicates photostimulation. *Middle*, waveforms of all detected events. Spikes from the single units are highlighted in red. Signal to noise ratio (SNR) is the peak-to-peak amplitude of the mean waveform divided by the standard deviation of the mean-subtracted noise. *Right*, histograms of the inter-spike-interval (ISI). False alarm rate (FA) is the fraction of spikes with ISI less than 2.5 ms.
- (B) ISI distribution from 32 randomly selected single units, rank ordered by FA. Red shading shows regions with $ISI < 2.5$ ms.
- (C) Summary of SNR and FA for all single units. Dots correspond to individual single units. Units shown in (B) are highlighted by green circles.
- (D) *Left*, overlaid mean spike waveforms for fast spiking GABAergic neurons (FS, putatively parvalbumin-positive neurons, red, $n = 18$) and non-fast spiking neurons (pyramidal neurons and GABAergic non-fast spiking neurons, are referred as putative pyramidal neurons, ppyr, blue, $n = 106$). A small subset of single units with intermediate spike durations were not classified (black, $n = 9$). *Right*, histogram of spike widths. The plot is the same as Figure 2C, but includes unclassified units.
- (E) Responses to photostimulation. Responses were normalized to baseline (dash line). Dots correspond to individual single units. Units with significant firing rate changes relative to baseline ($p < 0.05$, two-tailed t -test) are highlighted by circles. Same color scheme as (D).

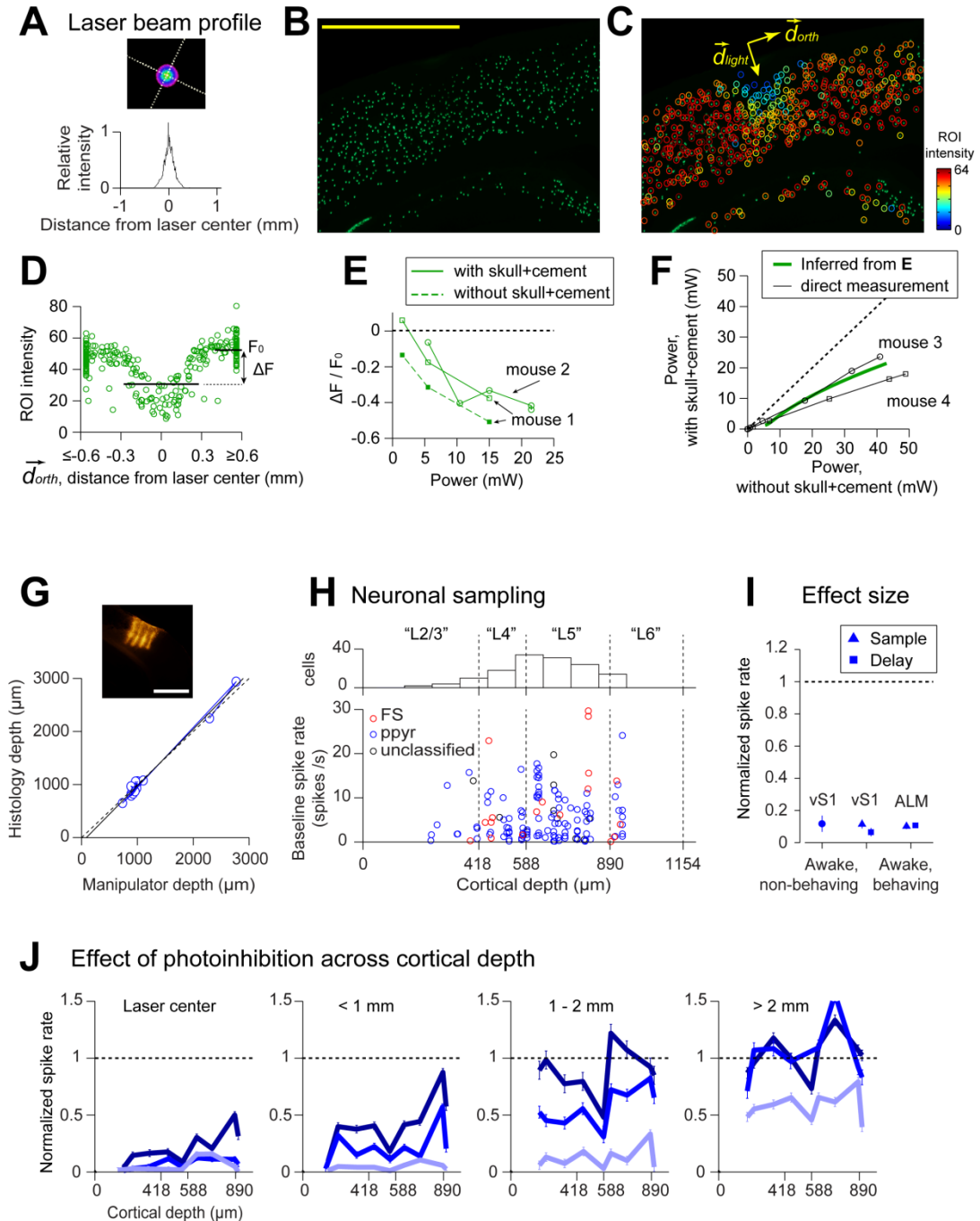


Figure S4 (related to Figure 2). Characterization of photoinhibition.

- (A) Spatial profile of the photostimulus at the surface of the skull. *Top*, profile of the laser beam. *Bottom*, laser intensity as a function of distance from laser center. $4\sigma = 0.4$ mm.
- (B) Photobleaching assay measuring the spread of blue light in the neocortex and light transmission through the clear-skull cap. Photobleaching was induced in a transgenic mouse line expressing GFP in the nuclei of a

- subset of neurons (*Rosa-LSL-H2B-GFP* crossed to *PV-IRES-Cre*) at different laser powers with and without the clear-skull cap (Experimental Procedures). Coronal section showing an example photobleaching site. Light dose, 21mW over 600 seconds. Scale bar, 1mm.
- (C) GFP intensity was measured in regions of interest (ROI) around individual nuclei (same image as in B). Circles, individual ROIs; $\overrightarrow{d_{light}}$, direction of the laser beam; $\overrightarrow{d_{orth}}$, direction normal to the laser beam.
- (D) Nuclear intensity as a function of distance from the laser center along $\overrightarrow{d_{orth}}$ (same data as B; all ROIs within 270 μm of the laser center along $\overrightarrow{d_{light}}$). F_0 , baseline ROI intensity, computed by averaging all ROIs > 440 μm away from the laser center. ΔF , ROI intensity change caused by photobleaching, computed by averaging all ROIs within 270 μm of the laser center and subtracting F_0 .
- (E) Photobleaching ($\Delta F / F_0$) at various laser powers with and without the clear-skull cap. Individual data points correspond to individual photobleaching sites. Measurements were made in 2 mice. Photobleaching was twice as fast without the clear-skull cap compared to with cap.
- (F) Light transmission obtained from the *in vivo* photobleaching assay (green line, inferred from E) and by direct measurements (black lines). In direct measurements laser power was measured before and after passing through isolated clear-skull caps (2 mice). The slopes of the curves indicate a transmission of 47%.
- (G) Reconstructing single unit recording depth. Recording depths of single units were determined from the electrode depth and the position of the recording sites on the silicon probe (www.neuronexus.com). Electrode depth was inferred from the manipulator depth. Actual electrode depth was tightly coupled to the depth reported by the manipulator. *Top*, Dil marking showing the recording track by a 4-shank silicon probe. Histology depth was measured based on the Dil marking. *Bottom*, the relationship between the manipulator depth and the actual electrode depth recovered from histology. Each dot correspond to a single recording penetration ($n = 13$).
- (H) Neuronal sampling across cortical depth. The definition of cortical layer ("L") boundaries was based on mouse brain atlas of vS1 (O'Connor et al., 2010 b). *Bottom*, baseline firing rate as a function of cortical depth. Circles correspond to individual vS1 single units recorded under awake, non-behaving condition ($n = 133$). Red, FS neurons; blue, putative pyramidal (ppyr) neurons; black, unclassified neurons.

- (I) Photoinhibition has similar effect size under non-behaving and behaving conditions, and across cortical areas. Normalized spike rate for ppyr neurons recorded from vS1 under awake non-behaving conditions ($n = 106$, circle); and from vS1 ($n = 35$) and ALM ($n = 101$) under behaving conditions (triangle, sample epoch; square, delay epoch). Error bars show s.e.m. over neurons.
- (J) Normalized spike rate across depth at various distances from the laser center for three laser powers (dark blue, 0.5 mW; blue, 1.5 mW; light blue 14 mW). Data from vS1 awake, non-behaving condition. *Top*, FS neurons ($n = 18$). *Bottom*, ppyr neurons ($n = 106$). Error bars show s.e.m. over neurons.

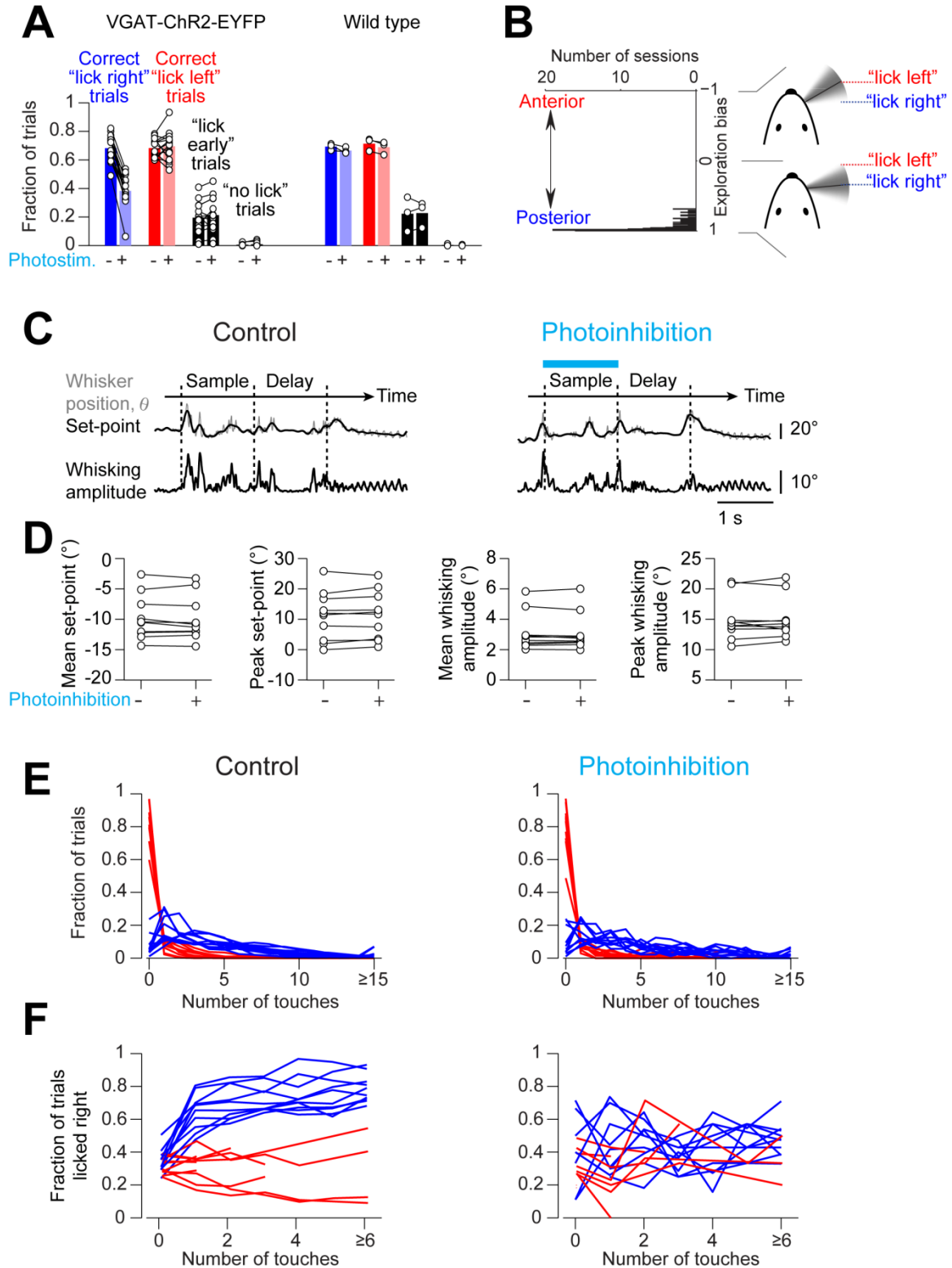


Figure S5 (related to Figure 3). Photoinhibition of vS1 does not change whisking nor the number of touches during object location discrimination.

- (A) Photostimulation without ChR2 expression does not cause behavioral changes. Performance in control trials and under vS1 photostimulation. *Left*, mice expressing ChR2-YFP in GABAergic neurons. Re-plot of data in Figure 3C. *Right*, photostimulation in three wild-type mice (C57Bl/6CrI) not expressing ChR2.
- (B) Mice used a highly asymmetric whisking strategy to solve the task. Exploration bias for 136 behavioral sessions from 11 mice. This represents the relative amount of time the whisker spent in the “posterior” pole position vs. the “anterior” pole position during the sample epoch, where $\text{bias} = (\text{“posterior”} - \text{“anterior”}) / (\text{“posterior”} + \text{“anterior”})$. Pole positions were defined by the whisker position, θ , at touch onset. Mice preferentially explored the “posterior” pole location (exploration bias > 0).
- (C) vS1 photoinhibition does not change whisker movements. Whisker movements in example “anterior” trials with (*right*) and without (*left*) vS1 photoinhibition. *Top*, trial structure and photoinhibition. *Middle traces*, whisker position (azimuthal angle, θ , grey) and set-point (black). *Bottom traces*, whisking amplitude (see Supplemental Experimental Procedures).
- (D) Summary data across mice ($n = 10$). Thin lines, individual mice. Mean set-point, mean whisking amplitude, peak set-point, and peak whisking amplitude were computed within the sample epoch (see Supplemental Experimental Procedures). The analysis was restricted to the “anterior” trials in which whisker movements were less obstructed by touches with the pole.
- (E) Distribution of the number of touches per trial (same format as Figure 1F; $n = 10$). Photoinhibition does not affect the distribution of touches in both “posterior” (blue) and “anterior” (red) trials.
- (F) The fraction of “lick right” responses as a function of number of touches (same format as Figure 1G; $n = 10$). Performance drop in “lick right” trials during vS1 photoinhibition is not due to changes in the number of touches.

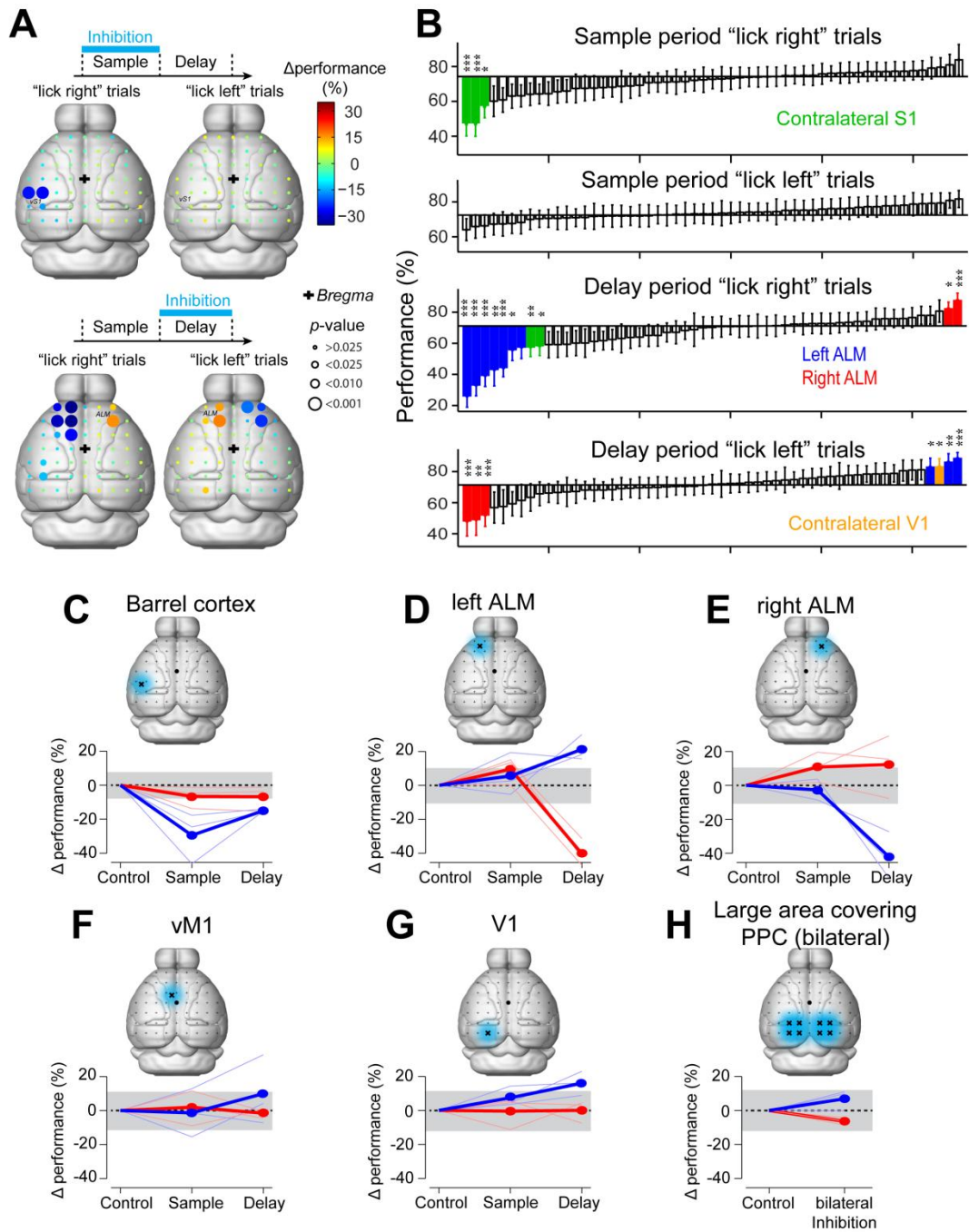


Figure S6 (related to Figure 4). Photoinhibition mapping.

(A) Photoinhibition during the sample (top) and delay (bottom) epochs. Same format as Figure 4B. The color at each photoinhibition location encodes the Δ performance from control performance. The size of the circles encodes the significance of performance changes.

(B) Performance when photoinhibiting different cortical regions, rank ordered and referenced to control performance. Error bars reflect standard errors

of the mean performance from bootstrap (see Experimental Procedures).
*, $p < 0.025$; **, $p < 0.01$; ***, $p < 0.001$.

- (C) *Top*, photoinhibition targeting vS1 (coordinates were based on intrinsic signal imaging of the C2 barrel column, Figure 3B). *Bottom*, performance change caused by photoinhibition during the sample and delay epochs. Thick lines, mean; thin lines, individual mice. Blues, “lick left” trials; red, “lick right” trials. Gray area shows the 95 % confidence interval for no change, estimated by bootstrapping the control condition. The experiment was carried out in 3 mice that learned the “lick left/ lick right” task with reversed contingency, where posterior pole position is associated with licking left. Same as Figure 5D.
- (D) Photoinhibition targeting left ALM (anterior 2.5mm, left 1.5mm from bregma).
- (E) Photoinhibition targeting right ALM (anterior 2.5mm, right 1.5mm).
- (F) Photoinhibition targeting vM1 (anterior 0.8mm, left 0.5mm).
- (G) Photoinhibition targeting V1 (posterior 3mm, left 2mm).
- (H) Bilateral photoinhibition targeting large areas overlapping PPC. Bilateral photoinhibition was deployed by rapidly (200Hz) scanning the laser between 8 grid-locations (posterior 2mm, lateral ± 1 mm, ± 2 mm; posterior 3mm, lateral ± 1 mm, ± 2 mm; 1.5mW mean laser power at each grid-location). For two mice, the photoinhibition was deployed throughout the whole trial (3.9 s). For the third mouse, the photoinhibition was only during the delay epoch. We did not observe any difference and the data were pooled.

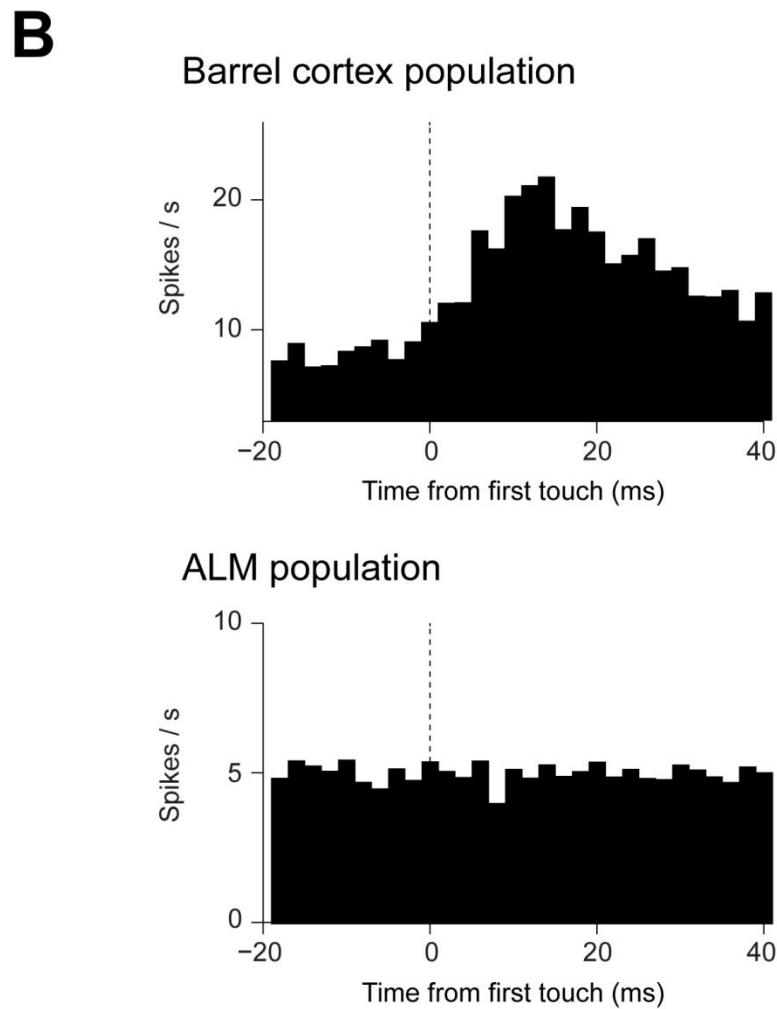
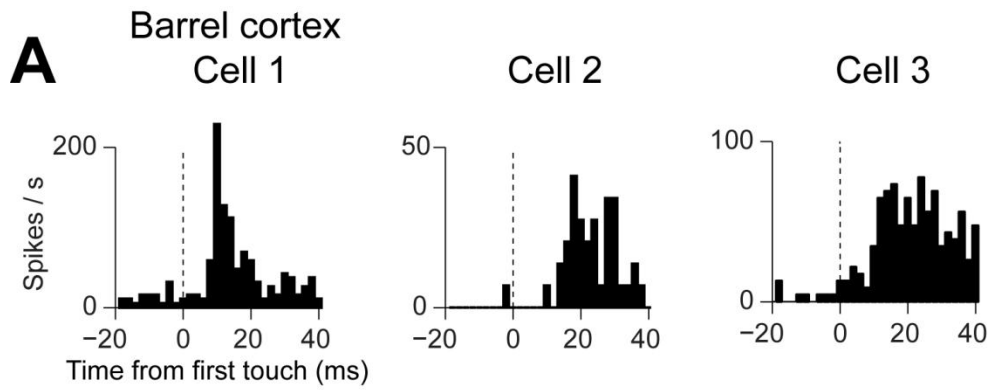


Figure S7 (related to Figure 6). Neurons in vS1 show touch-evoked responses.

(A) Three example neurons recorded in vS1 during object localization behavior. Responses are aligned to the first touch. Responses reflect

instantaneous spike rate binned in 2 ms windows. Neurons show touch-evoked responses approximately 10 ms after touch.

(B) vS1, but not ALM, showed touch-evoked responses. *Top*, population average of all the neurons recorded from vS1 ($n = 75$) aligned to first touch. *Bottom*, ALM population response ($n = 186$) aligned to first touch.

Table S1 (related to Figure 4). Performance changes and p -values in photoinhibition mapping.

Coordinates are relative to bregma (format: medial-lateral, anterior-posterior; negative values imply points on the left side of the brain or posterior to bregma). Δ performance is relative to control performance. P -values were obtained by bootstrapping (see Experimental Procedures). Bold font or red color indicates a significant performance change ($p < 0.025$, one tailed test). Red color indicates a significant performance change after correction for multiple comparisons (see Experimental Procedures).

Supplemental Experimental Procedures

Water Restriction & Surgical Procedures

Mice were housed in a 12:12 reverse light:dark cycle and tested during the dark phase. On days not tested in the behavior, mice received 1 mL of water (O'Connor et al., 2010a). On other days, mice were tested in experimental sessions lasting 1 to 2 hours where they received all their liquid (range, 0.5 to 2 mL). If mice did not maintain a stable body weight, they received supplementary water.

Mice were prepared for behavioral testing by implantation of a clear-skull cap (Figure 3B) and a headpost. The headpost was a custom made stainless steel or titanium bar 22.5 mm in length, 3.2 mm in width, with its bottom shaped to fit the shape of the skull. Aseptic surgical procedures were used during surgical procedures. Anesthetized mice (isoflurane, 1-2%) were kept on a thermal blanket (Harvard Apparatus) to maintain body temperature. The scalp and periosteum over the dorsal surface of the skull were removed. A layer of cyanoacrylate adhesive (Krazy glue, Elmer's Products Inc) was directly applied to the intact skull. The headpost was placed on the skull with its anterior edge aligned with the suture lambda (approximately over cerebellum) and cemented in place using clear dental acrylic (Jet Repair Acrylic; Lang Dental Manufacturing; P/N 1223-clear). A thin layer of clear dental acrylic was applied on top of the thin layer of cyanoacrylate adhesive which covered the entire exposed skull. Buprenorphine HCl (0.1 mg/kg, intraperitoneal injection; Bedford Laboratories) was used for postoperative analgesia. Ketoprofen (5 mg/kg, subcutaneous injection; Fort Dodge Animal Health) was used at the time of surgery and postoperatively to reduce inflammation. After the surgery, mice were allowed to recover for at least three days with free access to water before water restriction. Before experimentation (typically 1-8 weeks after the initial implantation of the headpost), the surface of the clear dental acrylic was polished using acrypoints (Acrylic Polishing Kit HP Shank, Pearson Dental). A thin layer of clear nail polish (Electron Microscopy Sciences, 72180) was then applied to reduce light glare.

For silicon probe recording, a small craniotomy (approximately 1.5 mm in diameter) was made over the recording site in mice already implanted with the clear-skull cap and headpost. The dental acrylic and bone were thinned using a dental drill. The remaining thinned bone was carefully removed using a bent forceps. A separate, smaller craniotomy (diameter, approximately 600 μ m) was made through the headpost bar for ground wires.

All neuronal recordings and photostimulation experiments were guided by intrinsic signal imaging (Figure 3B) (Masino et al., 1993). Mice were anesthetized with isoflurane (1%) after injection of chlorprothixene (0.007 mg, IM, ~0.36 mg/kg; Sigma C1671)

(Kaneko et al., 2008). The C2 whisker was stimulated with a piezo at 10 Hz. Images were acquired for 10 minutes directly through the clear-skull cap (Figure 3B).

Behavioral Training

Mice were trained to perform object location discrimination through operant conditioning (O'Connor et al., 2010a). In the first behavioral session, naïve mice were acclimatized to head-fixation and received liquid rewards simply by licking either lickport. The auditory “response” cue was played immediately before water delivery; this contingency was kept constant throughout training. As soon as mice learned to lick for water (~20-40 rewards), the reward scheme was changed to teach mice to sample both lickports. Specifically, only one lickport held a water reward. The rewarded lickport alternated between the two lickports after three rewards. Occasionally, manual water delivery was necessary to prompt the mice to lick from the other lickport. This phase of the training lasted for 1-3 sessions. Simultaneously, the vertical pole was also presented at the position corresponding to the rewarded lickport (e.g. if the rewarded lickport was the right-side lickport, the pole was presented to the mice at the posterior position, see Figure 1B). Presentation of the pole allowed the mice to gradually associate a pole position with licking from the correct lickport. Presentation of the pole at the posterior position always touched some of the whiskers, whereas presentation of the pole at the anterior position made fewer contacts. Often, mice would start to associate the pole with licking the correct lickport. Signs of this could be gauged by the observation that mice quickly switched to lick the right-side lickport when the pole was presented at the posterior position (which typically contacted their whiskers). Once such signs were observed, mice were subjected to the object location discrimination task with no delay epoch. In the object location discrimination task with no delay epoch, the presentation of the pole position was randomized. The mice were free to lick from the correct lickport immediately after the pole was presented to them. Licking before the “response” cue was not monitored and punished. Licking the incorrect lickport after the “response” cue led to no liquid reward and a brief time out. Typical mice learned the task quickly (~5 sessions, Figure S1). After mice reached criterion performance with full whisker fields (typically >75% correct), the delay epoch was introduced. First, mice were trained to lick only after the “response” cue. Licking before the “response” cue triggered an “alarm” sound from a siren buzzer and a brief timeout. Mice gradually learned to suppress their licking before the “response” cue was given. Once mice learned to contingent their licking on the “response” cue, the pole was removed at the end of the sample epoch and the delay epoch was added in incremental steps (steps of 0.2-0.4 sec). After mice achieved reasonable performance on the full object location discrimination task with delay (> 70%), their whiskers were progressively trimmed to a single whisker (full whiskers→C row→C2). The total training time to criterion performance (> 70 % correct)

was 3-4 weeks (Figure S1). The position of the lickport relative to the mice had a large effect on response bias. We ensured that the lickport position was unchanged between experimental sessions, with occasional modifications to counter bias.

Hardware & software

The hardware and software used for behavioral control was largely as described in O'Connor et al., 2010a. The entire apparatus was mounted on a vibration-isolation table (TMC; P/N 63-533) and enclosed in a custom light isolation box. The vertical pole was a metal pin (0.9 mm diameter) mechanically coupled to a linear slider (Schneeberger; P/N NDN 2-50.40) that controlled the anterior–posterior pole position with sub-micrometer resolution (Zaber; P/N NA08B30). This assembly was mounted on a pneumatic linear slider (Festo; SLS-10-30-P-A Mini slide; P/N 170496), connected to a compressed air source, and controlled by a solenoid valve (Festo; CPE 10-M1BH-5L-QS-6; P/N 196883). The pneumatic slider rapidly (0.2 s) brought the stimulus into and out of reach of the whiskers under computer control (see below).

A two-spout lickport made from 0.05-inch-diameter steel tubing was placed in front of the mouse, within reach of its tongue to deliver water rewards and record licks. Each of the two-spout lickport was electrically coupled to a custom build circuit board that detected licks *via* completion of an electrical circuit by the mouse's tongue (Slotnick, 2009). In addition, mouth movement was monitored using a photodiode under illumination of an infra-red laser diode (Thorlabs). Onset of licking (reaction time) was determined using the photodiode response. Liquid rewards were delivered under solenoid valve control (The Lee Company).

High speed video was taken at 1 kHz using Mikrotron Eosens Camera (Norpix, MC1362) to track the C2 whisker. A telecentric lens (Edmund Optics) focused a region of space (11.4mm x 15.2 mm) encompassing the two pole positions onto the camera chip (300 x 400 pixels). The frame acquisition of the high-speed camera was controlled by TTL pulses issued from another computer (see below). The video was recorded in Streampix 5 software (Norpix). Video acquisition always started before the initial movement of the vertical pole at the beginning of the trial, and lasted for 3-4.5 seconds through each trial. A 940 nm LED (Roithner Laser) provided background illumination for whisker imaging.

The behavioral apparatus was controlled by a software system (Z. Mainen, C. Brody, Cold Spring Harbor Laboratory, Cold Spring Harbor, NY) comprising MATLAB (Mathworks) routines communicating over the Ethernet with a real-time control system implemented in C on Linux using the RTLinux (www.rtlinux-gpl.org) or RTAI (www.rtai.org) kernel patches (C. Culianu). The real-time Linux system interfaced with valves and recorded licking responses using a PCI-6025E data acquisition board

(National Instruments) and the COMEDI drivers (www.comedi.org). A PCI-6713 data acquisition board controlled the photostimuli. The stepper motor was driven by commands sent through the serial port of the Windows computer running MATLAB. Timing of the high-speed video image frames was controlled by another computer running Ephus (www.ephus.org). Timing between the behavioral computer and the Ephus computer was synchronized using TTL pulses issued from RTLinux.

Photostimulation

Light from a 473 nm laser (DHOM-M-473-200, UltraLaser) was controlled by an acousto-optical modulator (AOM; MTS110-A3-VIS, Quanta Tech; extinction ratio 1:2000; 1 μ s rise time) and a shutter (Vincent Associates) (Figure 1A). The AOM provided analog control of laser intensity. Light exiting the AOM was connected using an FC/PC adaptor to a multimode optical fiber (62.5 μ m; Thorlabs) and a 2D scanning galvo system (GVSM002, Thorlabs; 0.5-5 ms step time for step size 0.57-35mm). The mirrors of the scanning system were controlled by RTLinux. Light from the galvo system passed through a beam expander (5x; plano-convex lenses LA1951-A and LA1384-A, Thorlabs) and was subsequently focused onto the brain surface with a $f = 200$ mm lens (AC508-200-A, Thorlabs). The laser had a Gaussian profile with a beam diameter of 400 μ m at 4σ at the position of brain surface (laser beam profiler, NT63-099, Edmundoptics, Figure S4). Laser power was calibrated using a handheld power meter (NT54-018, Edmundoptics). The scanning galvo system and AOM allowed simultaneous targeting of multiple non-adjacent cortical regions for photostimulation (Figure S6H).

To prevent the mice from distinguishing photostimulation trials from control trials using visual cues, a ‘masking flash’ pulse train (40 1ms pulses at 10 Hz) was delivered using a LED driver (Mightex, SLA-1200-2) and 470 nm LEDs (Luxeon Star) positioned near the eyes of the mice. The masking flash began as the pole started to move and continued through the end of the epoch in which photostimulation could occur. Mice were unable to solve the object location discrimination task using cues other than somatosensation. First, after trimming the C2 whisker performance dropped to chance level ($n = 3$) (Figure S1). Second, the behavioral box was kept dark so that the bright masking flash would be delivered to dark-adapted eyes and thus ‘blind’ the mice. Third, the masking flash was stroboscopic, minimizing visual motion cues.

Neuronal recordings

Extracellular spiking activity was recorded using silicon probes (NeuroNexus). For most sessions, we used 4 shanks probes with recording sites spaced 100 or 200 μ m apart (8 sites per shank, P/N A4x8-5mm-100-200-177, A4x8-5mm-100-200-413, A4x8-5mm-200-200-177, A4x8-5mm-200-200-413). In a few recording sessions, we also used

single-shank probes (P/N A1x32-Poly2-5mm-50s-177-A32; A1x32-Edge-5mm-20-177-A32; A1x32-6mm-50-177-A32). Silicon probes were connected to a custom headstage (Intan Technology) that multiplexed the 32-channel voltage recording into 2 analog signals (fabricated at Janelia Farm Research Campus, Brian Barbarits, Tim Harris, <http://www.janelia.org/lab/apig-harris-lab>). The multiplexed analog signals were recorded on a PCI6133 board at 312.5 kHz (National instrument) and digitized at 14 bit. The signals were demultiplexed into the 32 voltage traces at the sampling frequency of 19531.25Hz and stored for offline analyses in a custom software spikeGL (C. Cuianu, Anthony Leonardo, Janelia Farm Research Campus). The headstage was mounted on a motorized micromanipulator (MP-285, Sutter Instrument).

A 1-2 mm diameter craniotomy over the recording site was made prior to the recording sessions. For recordings under awake, non-behaving condition (Table 1), the craniotomy was made on the day of recording. The position of the craniotomy was 3.5 mm lateral and 1.5 mm posterior from bregma, in the barrel field. For recordings during active behavior, the craniotomy was made one day prior to the recording sessions. This minimized the discomfort of the animals and ensured high quality behavior during recording. The position of the craniotomy was guided by stereotactic coordinates for recordings in ALM (± 1.5 mm lateral from midline and 2.5 mm anterior of bregma) or intrinsic signal imaging for recordings in vS1 (in C2 and surrounding barrels).

Prior to each recording session, the tips of the silicon probe were brushed with DiI in ethanol solution and allowed to dry. The surface of the craniotomy was kept moist with saline. The silicon probe was positioned on the surface of the cortex and advanced manually into the brain at $\sim 3 \mu\text{m/s}$, normal to the pial surface. In our recording experiments, the depth of the electrode tip ranged from 749 to 1000 μm below the pial surface. The electrode depth was inferred from manipulator depth and verified with histology (Figure S4D). To minimize pulsation of the brain, a drop of silicone gel (3-4680, Dow Corning, Midland, MI, (Jackson and Muthuswamy, 2008)) was applied over the craniotomy after the electrode was in position. The tissue was allowed to settle for several minutes before the recording was started. The laser stimulus was manually positioned over the recording site for photostimulation during recording.

Histology

After the conclusion of experiments, mice were perfused transcardially with PBS followed by 4% PFA / 0.1 M PB. The brains were fixed overnight and sectioned. For the animals that underwent neuronal recording under non-behaving condition, coronal sections (100 μm) were cut. Images of DiI fluorescence were acquired on a macroscope (Olympus MVX10) and electrode tracks were compared to the manipulator depth reading

(Figure S4D). For mice that underwent neuronal recording during active behavior, the brain samples were sectioned differently in order to verify the recording locations. To verify the locations of silicon probes recordings in the barrel field, the brain was flattened between two glass slides. Tangential sections (100 μm) were cut and processed for cytochrome oxidase (CO). Images of DiI fluorescence within the CO-stained barrel map were acquired on a macroscope (Olympus MVX10). To recover the location of silicon probes in ALM, the cortex was sectioned coronally (100 μm) and imaged under the macroscope.

Two naïve *VGAT-ChR2-EYFP* mice were perfused, and their brains were sectioned and co-stained for anti-GFP (rabbit; Invitrogen A11122, 1:1,000 dilution) and anti-GAD67 (mouse; Invitrogen Mab5406, 1:1,000 dilution). Confocal images (Zeiss LSM 510) were acquired to examine ChR2 expression (Figure S2).

Data analysis

High-speed video of the C2 whisker was tracked using the Janelia Whisker Tracker (Clack et al., 2012) and analyzed to extract whisker position (azimuthal angle, θ), curvature, and contacts with the pole. Video frames with touch were identified semi-automatically based on proximity between the whisker and the pole, as well as whisker curvature changes induced by the pole. In sessions with electrophysiology, all contacts were further inspected manually. Whisker set-point (Figure S5) was the low-pass filtered (6-Hz) whisker angle. Whisking amplitude (Figure S5) was defined as the Hilbert transform of the absolute value of the band-pass filtered (6–60-Hz) whisker angle (Huber et al., 2012). To examine whisking during vS1 photoinhibition (Figure S5), set-point and whisking amplitude were measured for each trial.

To obtain spiking activity, the extracellular recording traces were preprocessed in 3 steps: first, raw voltage traces were band-pass filtered between 300 and 6,000 Hz (MATLAB ‘idealfilter’); second, common noise was estimated across channels by averaging channels at each time-point (MATLAB ‘trimmean’, using 50% of the channels), and this estimated common noise was subtracted from each of the individual channels; third, all events that exceeded an amplitude threshold of four standard deviations of the background activity were saved for subsequent spike sorting analyses. Event detection was done independently for each of the 32 channels.

Manual spike sorting was performed on all the saved events to extract single units. Initial spike clustering was performed in principal component space using automated software (UltraMegaSort2000, (Fee et al., 1996; Hill et al., 2011)). The clusters were further sorted manually in a data visualization tool MatClust (Karlsson and Frank, 2008): clusters were merged or separated, and cluster boundaries were manually adjusted to

include or exclude events near the cluster boundaries. Many clusters from the initial automated clustering contained multiple units that could not be resolved. These clusters were discarded. It was generally possible to isolate high-amplitude units from the background using cluster bounds defined in the PCA feature space. During a typical recording session (~1.5 hr), some units became separated from the background over time while others disappeared into the background. Only recording epochs in which a cluster was visibly separated from the background were saved (Figure S3). Finally, saved clusters were further evaluated by manually inspecting false alarm (FA) rate and miss rate. False alarm rate was estimated by examination of the inter-spike-interval (ISI) distribution, and units with excessive violation of the absolute refractory epoch were excluded (criteria: 0.5% events with $ISI < 2.5$ ms; a few FS neurons with $FA > 0.5\%$ were accepted, Figure S3). Miss rate was examined by plotting the sorted spiking events within the raw voltage traces (Figure S3). For each unit, voltage traces from a dozen of trials (randomly selected) trials were examined to assess the miss rate. Based on visual inspection, units with excessive misses were excluded. Because event detection was done independently for each of the 32 channels (see above), there was a possibility that the same unit could be recorded twice on two adjacent recording sites. For most of the recording sessions, this possibility was unlikely because we used recording configurations in which the adjacent recording sites were spaced at least 100 μm apart or more (see *Neuronal Recordings*). For a few sessions in which we used more closely spaced electrodes (20 or 50 μm recording sites spacing), we further inspected unit pairs recorded from those sessions. Specifically, we selected unit pairs with high synchronous firing rate ($> 20\%$) and discarded the lower quality unit (based on FA), if the unit pair had similar ISI distributions and peristimulus time histogram (PSTH). Overall, our recordings and analysis procedures yielded 7.2 putative single units per recording session (range, 1 to 17).

The anatomical depth of the single units was inferred based on micro-drive manipulator depth. Actual recording depth was calibrated for a subset of recording sessions in which the electrode was coated with DiI (see *Neuronal Recordings*). Actual recording depth was tightly coupled to the manipulator depth (Figure S4G). Actual recording depth was obtained from the manipulator depth and using the relationship in Figure S4G.

To quantify photoinhibition magnitude, we computed “normalized spike rate” during photostimulation (Figure 2E-F). For each neuron, we computed its firing rate during the photostimulus (1.3 s + 0.1 s ramp, Figure 2D) and its baseline firing rate (500 ms time window before photostimulus onset). The firing rates under photostimulation were averaged across the recorded ppyr population (without normalization) and normalized by dividing the averaged baseline firing rate. The “normalized spike rate” thus reports the total fraction of spiking output under photostimulation.

To quantify the onset time of photoinhibition (T_{on} , Figure 2D), we estimated the time when PSTH reached its minimum post stimulus onset (17.3 ± 1.4 ms, mean \pm s.e.m.; 1 ms bin). The quantification of photoinhibition offset time was complicated by two factors: first, the photostimulus was gradually reduced over 100ms at stimulus offset; second, a moderate amount of rebound activity occurred at stimulus offset. We therefore quantified the offset time of photoinhibition in two ways: first, we estimated the first time bin in which the population averaged PSTH reached its peak after stimulus offset (T_{off} , 124 ± 9.4 ms, mean \pm s.e.m.; 1 ms bin, Figure 2D); second, we estimated the first time bin in which the spike rate was no longer significantly different from background (50 ms bin; $p > 0.05$ two-tailed t -test; 255 ± 82.8 ms). Bootstrap was performed over neurons to obtain the standard errors.

References

- Clack, N.G., O'Connor, D.H., Huber, D., Petreanu, L., Hires, A., Peron, S., Svoboda, K., and Myers, E.W. (2012). Automated tracking of whiskers in videos of head fixed rodents. *PLoS computational biology* *8*, e1002591.
- Fee, M.S., Mitra, P.P., and Kleinfeld, D. (1996). Automatic sorting of multiple unit neuronal signals in the presence of anisotropic and non-Gaussian variability. *J Neurosci Methods* *69*, 175-188.
- Hill, D.N., Mehta, S.B., and Kleinfeld, D. (2011). Quality metrics to accompany spike sorting of extracellular signals. *J Neurosci* *31*, 8699-8705.
- Huber, D., Gutnisky, D.A., Peron, S., O'Connor, D.H., Wiegert, J.S., Tian, L., Oertner, T.G., Looger, L.L., and Svoboda, K. (2012). Multiple dynamic representations in the motor cortex during sensorimotor learning. *Nature* *484*, 473-478.
- Jackson, N., and Muthuswamy, J. (2008). Artificial dural sealant that allows multiple penetrations of implantable brain probes. *J Neurosci Methods* *171*, 147-152.
- Karlsson, M.P., and Frank, L.M. (2008). Network dynamics underlying the formation of sparse, informative representations in the hippocampus. *The Journal of neuroscience : the official journal of the Society for Neuroscience* *28*, 14271-14281.

Kaneko, M., Hanover, J.L., England, P.M., and Stryker, M.P. (2008). TrkB kinase is required for recovery, but not loss, of cortical responses following monocular deprivation. *Nature neuroscience* 11, 497-504.

Masino, S.A., Kwon, M.C., Dory, Y., and Frostig, R.D. (1993). Characterization of functional organization within rat barrel cortex using intrinsic signal optical imaging through a thinned skull. *Proceedings of the National Academy of Sciences of the United States of America* 90, 9998-10002.

O'Connor, D.H., Clack, N.G., Huber, D., Komiyama, T., Myers, E.W., and Svoboda, K. (2010a). Vibrissa-based object localization in head-fixed mice. *J Neurosci* 30, 1947-1967.

O'Connor, D.H., Peron, S.P., Huber, D., and Svoboda, K. (2010b). Neural activity in barrel cortex underlying vibrissa-based object localization in mice. *Neuron* 67, 1048-1061.

Slotnick, B. (2009). A simple 2-transistor touch or lick detector circuit. *J Exp Anal Behav* 91, 253-255.

Zhao, S., Ting, J.T., Atallah, H.E., Qiu, L., Tan, J., Gloss, B., Augustine, G.J., Deisseroth, K., Luo, M., Graybiel, A.M., *et al.* (2011). Cell type-specific channelrhodopsin-2 transgenic mice for optogenetic dissection of neural circuitry function. *Nature methods* 8, 745-752.